Surface Science 653 (2016) 45–54

Contents lists available at ScienceDirect

Surface Science

journal homepage: www.elsevier.com/locate/susc

# Adsorption of formate species on Cu(*h*,*k*,*l*) low index surfaces

Arunabhiram Chutia [a,b,*], Ian P. Silverwood [a,b], Matthew R. Farrow [b], David O. Scanlon [b,c], Peter P. Wells [a,b], Michael Bowker [a,d], Stewart F. Parker [a,e], C. Richard A. Catlow [a,b,d,*]

[a] UK Catalysis Hub, Research Complex at Harwell, Rutherford Appleton Laboratory, Didcot, OX11 0FA, UK
[b] University College London, Kathleen Lonsdale Materials Chemistry, 20 Gordon Street, London WC1H 0AJ, UK
[c] Diamond Light Source Ltd., Diamond House, Harwell Science and Innovation Campus, Didcot, Oxfordshire OX11 0DE, UK
[d] Cardiff Catalysis Institute, School of Chemistry, Cardiff University, Cardiff, CF10 3AT, UK
[e] ISIS Facility, STFC Rutherford Appleton Laboratory, Didcot, OX11 OFA, UK

ARTICLE INFO

*Article history:*
Received 22 January 2016
Received in revised form 28 April 2016
Accepted 5 May 2016
Available online 7 May 2016

*Keywords:*
Density functional theory
Inelastic neutron scattering spectroscopy
Formate stability
Charge transfer
Hybridization
Non-axial Cu *d*–orbital

ABSTRACT

We report a density functional theory study on the relative stability of formate species on Cu(*h*,*k*,*l*) low index surfaces using a range of exchange-correlation functionals. We find that these functionals predict similar geometries for the formate molecule adsorbed on the Cu surface. A comparison of the calculated vibrational transition energies of a perpendicular configuration of formate on Cu surface shows an excellent agreement with the experimental spectrum obtained from inelastic neutron spectroscopy. From the calculations on adsorption energy we find that formate is most stable on the Cu(110) surface as compared to Cu(111) and Cu(100) surfaces. Bader analysis shows that this feature could be related to the higher charge transfer from the Cu(110) surface and optimum charge density at the interfacial region due to bidirectional electron transfer between the formate and the Cu surface. Analysis of the partial density of states finds that in the –5.5 eV to –4.0 eV region, hybridization between O *p* and the non-axial Cu $d_{yz}$ and $d_{xz}$ orbitals takes place on the Cu(110) surface, which is energetically more favourable than on the other surfaces.



## 1. Introduction

Formate is a key stable intermediate, which is directly involved in many industrially important reactions for example in the synthesis of methanol from syngas ($H_2/CO_2/CO$) [1,2]. In this reaction, the formate species can be formed from $CO_2$ and $H_2$ and can be hydrogenated to methanol, which is believed to be the rate determining step [2]. Formate intermediates also play a crucial role in other catalytic processes, which include ethanol steam reforming, the water gas shift reaction and methanol synthesis on metal surfaces. Additionally, it is also relevant to gaining a fundamental understanding of the physicochemical processes occurring at the interfacial region between an organic molecule and the metal surface. It is therefore, of great interest to understand the detailed structural and electronic properties of adsorbed formate species on metallic surfaces and to clarify its crucial role in surface catalysis [3].

Experimentally, as early as the 1960s, chemisorption of formate species on metallic surfaces such as Ni(110) was reported by various workers [4,5]. These studies used a wide range of experimental techniques including Auger Electron Spectroscopy (AES), Low Energy Electron Diffraction (LEED), X-ray Photoelectron Spectroscopy (XPS), Ultra-violet Photoelectron Spectroscopy (UPS), Temperature-Programmed Desorption (TPD), Scanning Tunnelling Microscopy (STM), Near Edge X-ray Absorption Fine Structure (NEXAFS) and Neutron Vibrational Spectroscopy (INS) [2,4–9]. These techniques gave considerable information about the nature of the formate species on metallic surfaces and the kinetics of its formation by acid proton dissociation when adsorbed at low-temperature [6]. Many experiments were also devoted to understanding the geometry of adsorbed formate species. Crapper et al., for example, used NEXAFS to propose that formate upon adsorption adopts an upright orientation on the surface with the two oxygen atoms bound to adjacent metal atoms [10]. Later, Poulston et al. used INS to arrive at similar conclusions [11].

Several theoretical studies have been also undertaken to understand the electronic structure and the interaction between formate species and a metallic surface [12–14]. For these studies density functional theory (DFT) and semiempirical methods were employed on both periodic and cluster model approaches [15,16]. Gomes et al. for example, used cluster models for Cu(*h*,*k*,*l*) surfaces to study the interaction with formate species [13]. Similarly, Nakatsuji et al. used $Zn_4O_4$ in an embedded cluster approach to study the chemisorption and surface reaction of formate species [14]. Atodiresei et al. employed DFT on periodic models to study the arrangement of an adsorbed formate free radical on the Cu(110) surface [12]. HongYan et al. also used DFT for studying the

* Corresponding authors at: UK Catalysis Hub, RCaH, Rutherford Appleton Laboratory, Didcot, OX11 0FA, UK.

http://dx.doi.org/10.1016/j.susc.2016.05.002

most stable adsorption sites of formate species on (110) surfaces of various transition metals [17]. A detailed study on the interaction of formate species on Cu(*h*,*k*,*l*) low index surfaces was carried out by Hu et al. [18]. In this work, they used cluster models to examine the convergence of the adsorption properties with respect to their size to investigate the activity of Cu planes for formate species adsorption. In other work Morikawa et al. studied the adsorption of formate species on clean and Zn-deposited Cu(111) surface by using DFT [19]. Phillips et al. also reported preferred adsorption sites and other electronic properties of formate ions on Cu(110) surfaces using various quantum chemical methods [15]. While a plethora of information about formate species on metal and metal oxide surfaces has been generated, the local structure, and adsorption properties of formate species on Cu(*h*,*k*,*l*) surfaces are still not clearly understood.

Therefore, in the current study we have performed a periodic DFT study and carried out a direct comparison with experimental (INS) investigation to explore systematically and clarify the adsorption properties formate species with and without a co-adsorbed H atom on the low index Cu surfaces (Cu(111), Cu(110) and Cu(100)). Further to this, we have provided a detailed picture of the nature of formate (as free radical and anionic in nature), various modes of its adsorption and the nature of bonding on the Cu(*h*,*k*,*l*) index surfaces to clarify the nature of the interaction of the species with the Cu surface.

## 2. Computational details

We employed the Vienna Ab-initio Simulation Package (VASP) to perform DFT based calculations [20–23]. We used the projector augmented wave (PAW) method and the cut-off energy for the expansion of the plane-wave basis sets was set to 550 eV, which gave bulk energies converged to within $10^{-5}$ eV. We chose a convergence criterion of 0.01 eV/Å for our structural optimisations. For all the preliminary calculations, the most commonly used Perdew-Burke-Ernzerhof (PBE) version of the generalized gradient approximation (GGA) was used to carry out total energy calculations and perform geometry optimizations [24]. For the bulk calculations, the Brillouin zone was integrated using a Monkhorst-Pack (MP) grid of 11 × 11 × 11 k-points. The ideal Cu(111, 110 and 100) surfaces were modelled by a 3 × 3 (referred to as $Cu_{3x3}$ models) and 4 × 4 (referred to as $Cu_{4\times4}$ models) supercell with 5 and 7 atomic layers respectively from bulk copper with an experimental lattice constant of 3.615 Å and a k-point grid of 4 × 4 × 1 [25]. During the optimization process, we relaxed the entire system, which consisted of formate free radical (i.e., uncharged HCOO subsequently referred to as formate) and the Cu(*h*,*k*,*l*) surfaces. In our models we placed the formate on both sides of the copper surface so as to nullify the dipole moments that would be present in the single-sided system. For comparative purposes, we also used other GGA functionals: PW91 and PBEsol [26,27]. To check the influence of dispersive forces, we used Grimme's D2 corrections together with the PBE exchange-correlation functional [28]. The adsorption energy of formate on Cu(*h*,*k*,*l*) low index surface was calculated using:

$$E_{ad} = \{E_{formate+Cu(h,k,l)} - (E_{cu(h,k,l)} + 2 \times E_{formate})\}/2, \quad (1)$$

where, $E_{ad}$ is the adsorption energy, $E_{formate\ +\ Cu(h,k,l)}$ is the energy of the system with the formate adsorbed on Cu surfaces, $E_{Cu(h,k,l)}$ is the energy of pristine surface and $E_{formate}$ is the energy of the formate. In realistic systems, the adsorption of formate may be accompanied by co-adsorption of H atoms. Therefore, we also considered the same models with an H atom co-adsorbed with the formate on Cu(*h*,*k*,*l*) surfaces. Previous detailed theoretical studies on the adsorption of H atoms on Cu(*h*,*k*,*l*) surfaces have shown that H atoms are more stable on the 3-fold fcc site for Cu(111), on the short bridge site for Cu(110) and the 4-fold HCP site on Cu(100) surface [29–31]. Thus, for the co-adsorbed systems we adopted the configuration of perpendicular formate geometry along with an H atom in the sites mentioned above. The adsorption energy was calculated using:

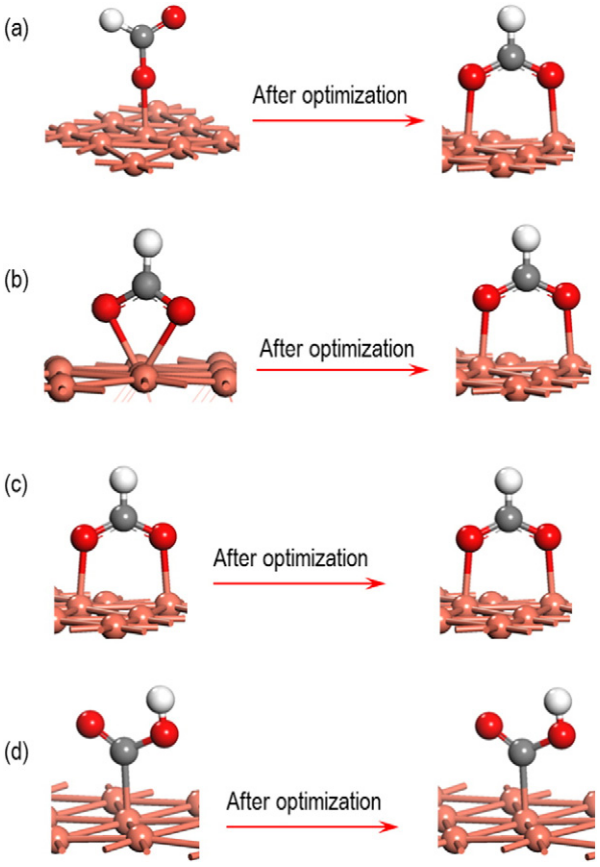


**Fig. 1.** Formate adsorbed on Cu(111) surface through (a) one O-atom, (b) two O-atoms on the same Cu atom, (c) two O-atoms on two different Cu atoms and (d) C-atom on a Cu atom.

$$E_{ad} = \{E_{H+formate+Cu(h,k,l)} - (E_{cu(h,k,l)} + 2 \times E_{formic\ acid})\}/2, \quad (2)$$

where $E_{ad}$ is the adsorption energy, $E_{H\ +\ Formate\ +\ Cu(h,k,l)}$ is the energy of formate co-adsorbed with a H atom on the Cu(*h*,*k*,*l*) surface, $E_{Cu(h,k,l)}$ is energy of the pristine Cu surface and $E_{formic\ acid}$ is the energy of isolated

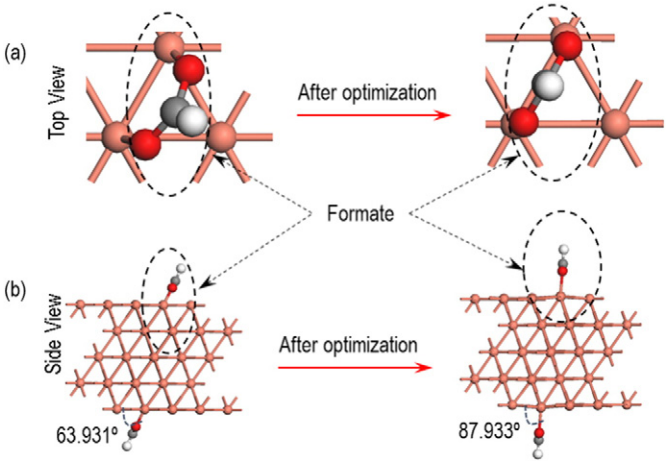


**Fig. 2.** (a) Top view and (b) side view of formate slanted at an angle of 63.931° before optimization and adopting an angle of 87.933° after optimization.

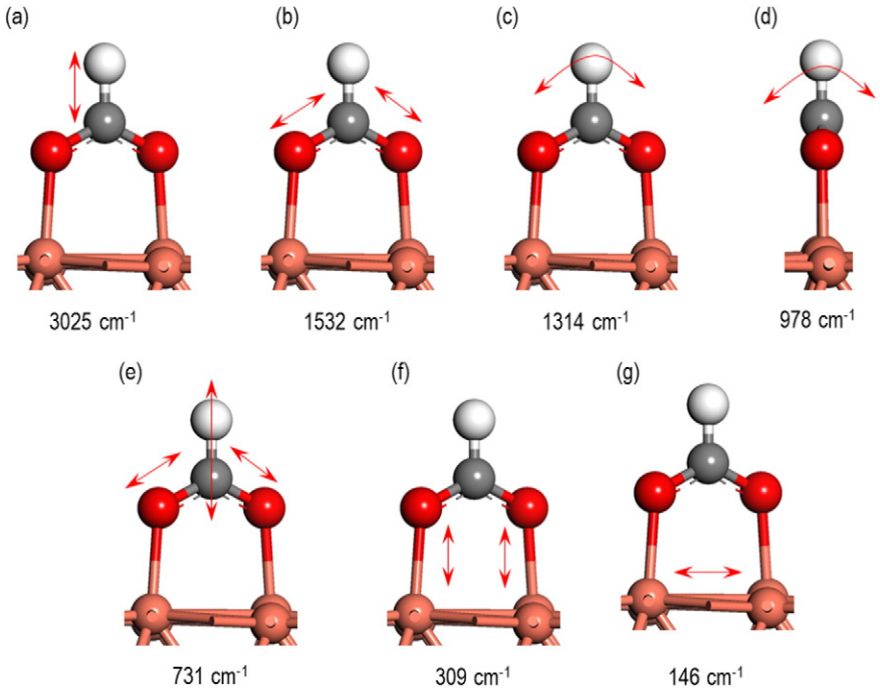


**Fig. 3.** Vibrational frequencies due to (a) C–H stretching, (b) O–C assymmetric stretching, (c) in-plane C–H stretching, (d) out of plane C–H stretching, (e) C–H stretching due to O–C symmetric stretching, (f) O–Cu symmetric stretching and (g) Cu–Cu stretching.

formic acid. In addition, we also modelled the adsorption of formic acid directly on the Cu surface, which is discussed later.

The charges on various atoms were obtained using the Bader charge analysis as implemented by Henkelman and co-workers [32]. The charge density difference, $\rho_{diff}$, was calculated by subtracting the sum of the charge densities of formate and the pristine geometry of the surface of the same geometry from the total charge density of the system i.e., formate adsorbed on Cu(*h*,*k*,*l*) using the equation:

$$\rho_{diff} = \rho_{total} - \left(\rho_{Pristinesurface} + \rho_{molecule}\right) \quad (3)$$

The climbing-image nudged elastic band (NEB) method was used to determine the minimum energy path for evaluating the activation energy barrier for the abstraction of H from HCOOH on the Cu(111) surface [33,34]. For these calculations, a four-layered Cu(111) slab with 3 × 3 surface unit cell and six equivalent layers of vacuum between two successive metal slabs is used. To reduce the computational cost during the NEB calculations the adsorption is allowed on only one of the two surfaces with a cutoff energy of 450 eV, energy convergence of $10^{-5}$ eV and a convergence criterion of 0.02 eV/Å for structural optimisations. The dipole moment for these calculations, due to the adsorbed species, is accounted for using the methods as implemented in VASP according to the works of Makov et al. and Neugebauer et al. [35,36]. The bottom two-layers are fixed to mimic the bulk of the system.

In addition to the above calculations on formate free radical species, we further extended this study to understand the effect of formate as an ion. These calculations were performed using the PBE version of GGA by placing a $Na^+$ ion near the formate on a three-fold hollow site, long-bridge site and four-fold hollow site for Cu(111), Cu(110) and Cu(100) 4 × 4 supercell models. A k-point grid of 2 × 2 × 1 was used. The adsorption energy ($E_{ad}$) of formate on Cu(*h*,*k*,*l*) in the presence of $Na^+$ in a low index surface was calculated using:

$$E_{ad} = \left\{E_{formate+Na^+ + Cu(h,k,l)} - \left(E_{cu(h,k,l)} + 2 \times E_{formate} + 2\, E_{Na}\right)\right\}/2 \quad (4)$$

where, $E_{formate\ +\ Na^+ +\ Cu(h,k,l)}$ is the energy of the system with the formate co-adsorbed with $Na^+$ ion on Cu surfaces, $E_{Cu(h,k,l)}$ is the energy of pristine surface, $E_{formate}$ is the energy of the formate and $E_{Na}$ is the energy of a Na ion.

To generate INS spectra to compare with experimental data, some of the calculations were repeated using the plane wave pseudopotential CASTEP code [37] (PBE functional [20], 880 eV plane wave cut-off, 4 × 4 × 1 Monkhorst-pack grid, 10 Å vacuum gap) and the output implemented in to the procedure in ACLIMAX [38].

## 3. Results and discussion

### 3.1. Denticity and perpendicularity of formate molecule

DFT calculations were firstly performed to clarify the preferred mode of bonding of formate to the surface: 1) O–monodenticity (formate bonded to the Cu-surface through an O atom), 2) O–bidenticity (both

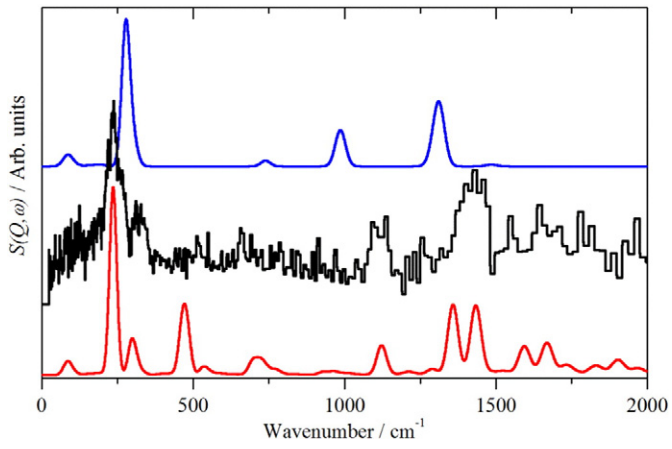


**Fig. 4.** Comparison of the experimental INS spectrum of formate adsorbed on a reduced CuO surface (which creates a thick layer of Cu metal) (middle trace) and the calculated INS spectra of formate adsorbed on a Cu(111) surface. Top trace: as generated from the calculation of formate + H on Cu(111) (the intensities of the modes of the co-adsorbed H have been set to zero) 0 → 1 transitions only. Bottom trace: data in the top trace after scaling the modes and inclusion of all overtones and combinations up to 0 → 10.

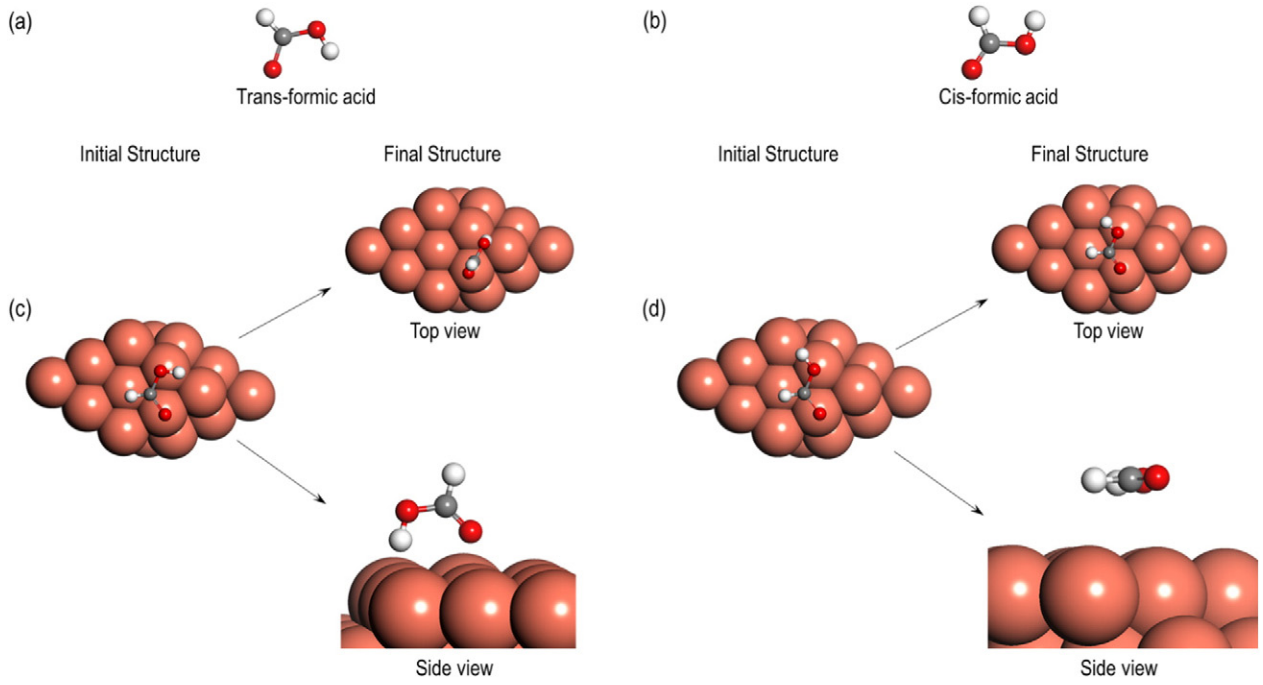


**Fig. 5.** (a) Formic acid with H atoms trans to each other, (b) formic acid with H atoms cis to each other, (c) trans-formic acid before and after geometrical optimization and (d) cis-formic acid before and after geometrical optimization.

the O atoms of formate bonded to the same Cu-atom), 3) O–bidenticity (the O atoms bonded to two different Cu atoms) and 4) C–monodenticity (formate molecule bonded to the Cu surface through the C atom) (see Fig. 1). After relaxation of all these structures, the monodentate and bidentate formate bonded through O atoms converged to a bidentate geometry with the formate oxygen atoms bonded to adjacent copper atoms. However, for the structure with C–monodenticity, the geometry remains the same. To see which one of these two configurations was the most favourable, the adsorption energy ($E_{ad}$) for O-bidentate (Fig. 1(c)) and C-monodentate structure (Fig. 1(d)) was considered. We find that $(E_{ad})_{O\text{-bidentate}}$ was −0.895 eV lower in energy than the $(E_{ad})_{C\text{-monodentate}}$, showing the O-bidentate structure was the lowest energy geometry for formate on a Cu surface. We also checked if formate on a Cu(*h*,*k*,*l*) surface would adopt a tilted or a perpendicular geometry. For this a random initial angle of ~64° for formate with respect to the Cu(111) surface was chosen (Fig. 2). After optimization, the formate adopted an angle of ~88° indicating that the bidentate formate molecule on Cu surfaces is most stable in a perpendicular geometry. Our calculations therefore confirm the perpendicular geometry with the bidentate configuration,

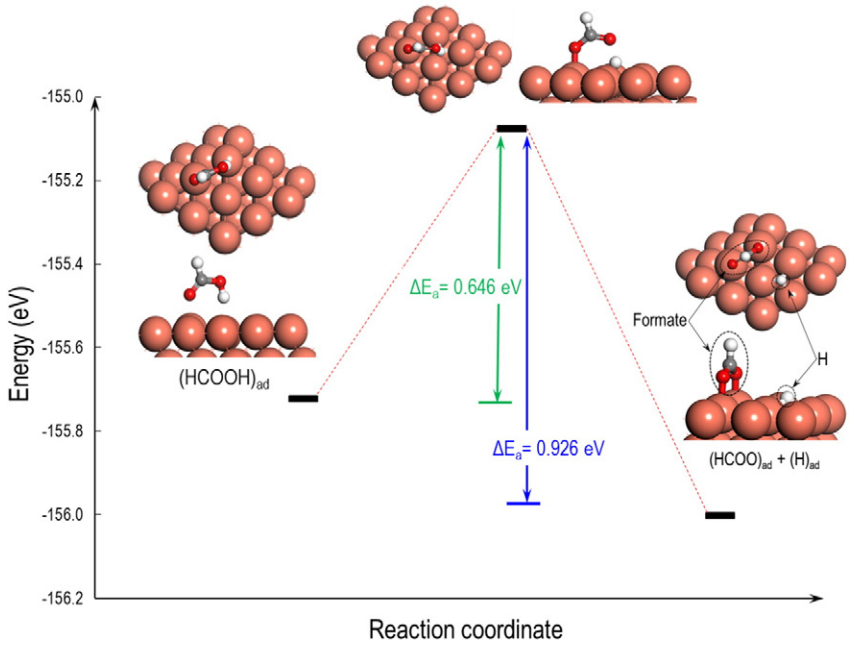


**Fig. 6.** Illustration of the activation energy barrier for H abstraction from formic acid on the Cu(111) surface.

**Table 1**
Bond lengths calculated for formate adsorbed on Cu(*h*,*k*,*l*) using PW91, PBE, PBE-D2 and PBEsol exchange-correlation functional. Here "blk" refers to bulk and "srf" refers to surface.

| Systems | $(Cu\text{-}Cu)_{blk}$ | | | | $(Cu\text{-}Cu)_{srf}$ | | | | O–Cu | | | |
|---|---|---|---|---|---|---|---|---|---|---|---|---|
| | PW91 | PBE | PBE-D2 | PBEsol | PW91 | PBE | PBE-D2 | PBEsol | PW91 | PBE | PBE-D2 | PBEsol |
| $100_{Pristine}$ | 2.556 | 2.556 | 2.556 | 2.556 | 2.556 | 2.556 | 2.556 | 2.556 | – | – | – | – |
| $100_{formate}$ | 2.542 | 2.540 | 2.543 | 2.541 | 2.551 | 2.541 | 2.574 | 2.577 | 1.995 | 1.999 | 1.989 | 1.953 |
| $110_{Pristine}$ | 2.556 | 2.556 | 2.556 | 2.556 | 2.556 | 2.556 | 2.556 | 2.556 | – | – | – | – |
| $110_{formate}$ | 2.555 | 2.557 | 2.557 | 2.558 | 2.551 | 2.549 | 2.561 | 2.562 | 1.973 | 1.975 | 1.969 | 1.934 |
| $111_{Pristine}$ | 2.556 | 2.556 | 2.556 | 2.556 | 2.556 | 2.556 | 2.556 | 2.556 | – | – | – | – |
| $111_{formate}$ | 2.562 | 2.559 | 2.556 | 2.553 | 2.545 | 2.546 | 2.564 | 2.571 | 2.013 | 2.017 | 2.009 | 1.971 |
| Systems | O–C | | | | C–H | | | | O–H | | | |
| | PW91 | PBE | PBE-D2 | PBEsol | PW91 | PBE | PBE-D2 | PBEsol | PW91 | PBE | PBE-D2 | PBEsol |
| $100_{formate}$ | 1.270 | 1.270 | 1.270 | 1.267 | 1.107 | 1.108 | 1.108 | 1.111 | 2.019 | 2.020 | 2.021 | 2.020 |
| $110_{formate}$ | 1.269 | 1.270 | 1.270 | 1.266 | 1.106 | 1.108 | 1.108 | 1.111 | 2.018 | 2.019 | 2.020 | 2.019 |
| $111_{formate}$ | 1.269 | 1.270 | 1.270 | 1.267 | 1.106 | 1.108 | 1.108 | 1.111 | 2.017 | 2.019 | 2.020 | 2.019 |

**Table 2**
Bond lengths calculated for formate and an H atom adsorbed on Cu(*h*,*k*,*l*) using PW91, PBE, PBE-D2 and $PBE_{Sol}$ exchange-correlation functional. Here "blk" refers to bulk and "srf" refers to surface.

| Systems | $(Cu\text{–}Cu)_{blk}$ | | | | $(Cu\text{–}Cu)_{srf}$ | | | | O–Cu | | | |
|---|---|---|---|---|---|---|---|---|---|---|---|---|
| | PW91 | PBE | PBE-D2 | PBEsol | PW91 | PBE | PBE-D2 | PBEsol | PW91 | PBE | PBE-D2 | PBEsol |
| $100_{formate}$ | 2.549 | 2.553 | 2.568 | 2.561 | 2.545 | 2.576 | 2.583 | 2.578 | 1.995 | 1.999 | 1.99 | 1.955 |
| $110_{formate}$ | 2.553 | 2.556 | 2.556 | 2.545 | 2.559 | 2.569 | 2.575 | 2.571 | 1.967 | 1.971 | 1.962 | 1.93 |
| $111_{formate}$ | 2.555 | 2.56 | 2.559 | 2.565 | 2.555 | 2.557 | 2.560 | 2.565 | 2.014 | 2.019 | 2.006 | 1.971 |
| Systems | C–H | | | | O–C | | | | $H_{ad}$ –Cu | | | |
| | PW91 | PBE | PBE-D2 | PBEsol | PW91 | PBE | PBE-D2 | PBEsol | PW91 | PBE | PBE-D2 | PBEsol |
| $100_{formate}$ | 1.106 | 1.108 | 1.108 | 1.111 | 1.27 | 1.27 | 1.271 | 1.267 | 1.877 | 1.877 | 1.878 | 1.861 |
| $110_{formate}$ | 1.106 | 1.107 | 1.107 | 1.111 | 1.269 | 1.27 | 1.271 | 1.267 | 1.645 | 1.647 | 1.641 | 1.634 |
| $111_{formate}$ | 1.106 | 1.108 | 1.107 | 1.111 | 1.27 | 1.27 | 1.271 | 1.267 | 1.744 | 1.747 | 1.736 | 1.734 |

on which we now concentrate for the remainder of this study of formate on Cu(*h*,*k*,*l*) surfaces.

In addition, we compared the calculated vibrational transition energies of the perpendicular geometry of formate on a Cu surface with the experimental data [10]. The vibrational modes and their corresponding values are shown in Fig. 3. The C–H stretch occurs at 3025 $cm^{-1}$; the OCO asymmetric stretching is observed at 1532 $cm^{-1}$, the in-plane and out-of-plane C–H bending modes are seen at 1314 $cm^{-1}$ and 978 $cm^{-1}$ respectively. The OCO scissor mode occurs at 731 $cm^{-1}$ and the O–Cu and Cu–Cu stretching are observed at 309 $cm^{-1}$ and 146 $cm^{-1}$ respectively. Fig. 4 compares the INS spectra (top and bottom traces in Fig. 4) calculated for the formate – Cu(111)/H system (see Fig. 5) with a previously reported spectrum (Fig. 4 middle trace) of formate on a reduced CuO surface, that generates a thick layer of Cu metal [10]. The adsorbed H is calculated to have strong modes at 767, 781 and 841 $cm^{-1}$; the experimental spectrum has no evidence for these modes so their intensity was set to zero. We see that the calculated spectrum of the formate moiety (top trace in Fig. 4) gives a pattern of intensities and positions that are close to those observed experimentally. By shifting the transition energies of the calculated peaks to the experimental values (in essence scaling the energies) and inclusion of the higher order transitions (overtones and combinations, which are allowed transitions in the harmonic approximation for INS spectroscopy), excellent agreement with the

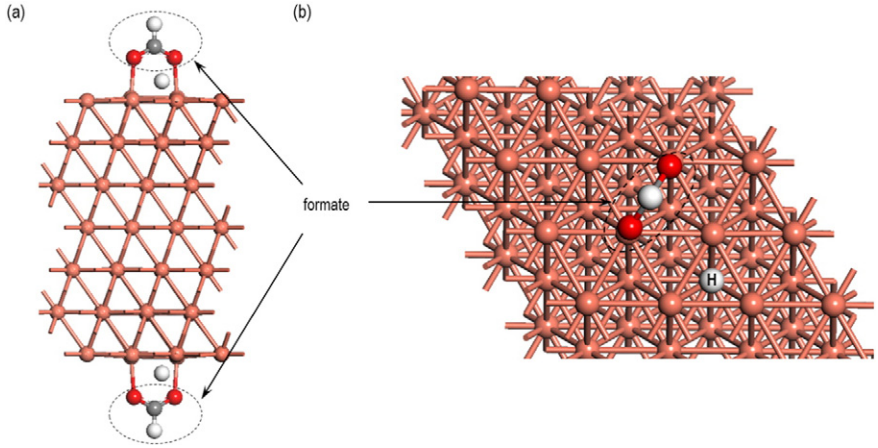


**Fig. 7.** (a) Side view and (b) top view of formate co-adsorbed with a H atom on the Cu(111) surface.

**Table 3**
Bond lengths calculated for formate and an H atom adsorbed on Cu(*h,k,l*) with 112 Cu atoms using PW91, PBE, PBE-D2, and $PBE_{Sol}$ exchange-correlation functional. Here "blk" refers to bulk and "srf" refers to surface.

| Systems | $(Cu\text{-}Cu)_{blk}$ | | | | $(Cu\text{–}Cu)_{srf}$ | | | | O–Cu | | | |
|---|---|---|---|---|---|---|---|---|---|---|---|---|
| | PW91 | PBE | PBE-D2 | PBEsol | PW91 | PBE | PBE-D2 | PBEsol | PW91 | PBE | PBE-D2 | PBEsol |
| $100_{Clean}$ | 2.556 | 2.556 | 2.556 | 2.556 | 2.556 | 2.556 | 2.556 | 2.556 | – | – | – | – |
| $100_{formate}$ | 2.559 | 2.551 | 2.559 | 2.561 | 2.551 | 2.540 | 2.571 | 2.568 | 1.991 | 1.995 | 1.985 | 1.948 |
| $110_{Clean}$ | 2.556 | 2.556 | 2.556 | 2.556 | 2.556 | 2.556 | 2.556 | 2.556 | – | – | – | – |
| $110_{formate}$ | 2.556 | 2.556 | 2.557 | 2.557 | 2.560 | 2.557 | 2.561 | 2.563 | 1.966 | 1.970 | 1.963 | 1.928 |
| $111_{Clean}$ | 2.556 | 2.556 | 2.556 | 2.556 | 2.556 | 2.556 | 2.556 | 2.556 | – | – | – | – |
| $111_{formate}$ | 2.557 | 2.557 | 2.560 | 2.552 | 2.545 | 2.557 | 2.562 | 2.562 | 2.011 | 2.015 | 2.005 | 1.968 |
| Systems | O–C | | | | C–H | | | | $H_{ad}$-Cu | | | |
| | PW91 | PBE | PBE-D2 | PBEsol | PW91 | PBE | PBE-D2 | PBEsol | PW91 | PBE | PBE-D2 | PBEsol |
| $100_{formate}$ | 1.269 | 1.270 | 1.271 | 1.267 | 1.106 | 1.108 | 1.108 | 1.111 | 1.877 | 1.878 | 1.880 | 1.862 |
| $110_{formate}$ | 1.269 | 1.270 | 1.271 | 1.267 | 1.106 | 1.107 | 1.107 | 1.110 | 1.646 | 1.648 | 1.642 | 1.634 |
| $111_{formate}$ | 1.269 | 1.270 | 1.271 | 1.267 | 1.106 | 1.108 | 1.108 | 1.111 | 1.745 | 1.747 | 1.740 | 1.736 |

experimental spectrum is obtained, validating the computational model and thus strongly suggests that the species observed experimentally is indeed the formate radical modelled in this study.

### 3.2. Formic acid on Cu(h,k,l) surfaces

The above analysis combined with INS spectroscopy gives a reliable model for investigating the detailed geometrical and electronic structure of formate on Cu(*h,k,l*). However, it is important to address the nature of the interaction of formic acid with a Cu surface and the energy barrier for the abstraction of H from HCOOH to give the formate species. To this end, as shown in Fig. 5 (a and b), we considered two different configurations of formic acid i.e., trans-formic acid (Fig. 5(a)) and cis-formic acid (Fig. 5(b)). In trans-formic acid, the two H-atoms are on different sides of the C–$O_H$ bond, while in the cis-formic acid, both the H-atoms are in the same side of the C–$O_H$ bond. We relaxed the geometries with the parallel conformations of trans/cis formic acid over Cu(111) (Fig. 5(c–d)). On the fully relaxed geometries the trans-formic acid is adsorbed perpendicular to the Cu(111) surface with the H of the OH group facing the surface and in the case of cis-formic acid it remains parallel to the surface. Calculation of adsorption energies on these systems shows that trans-formic acid ($E_{ad} = -0.193$ eV) is more stable than cis-formic acid ($E_{ad} = -0.094$ eV) on the Cu(111) surface by −0.099 eV. The adsorption energies also shows that formic acid is very weakly adsorbed on the Cu(111) surface. Based on these findings we used the NEB method to calculate the activation energy barrier for the abstraction of H from HCOOH for the trans-formic acid i.e.,

$$(HCOOH)_{ad} \rightleftharpoons (HCOO)_{ad} + (H)_{ad} \quad (5)$$

We saw that the energy barrier for the abstraction of proton from trans-formic acid is 0.646 eV and the reaction is exothermic by −0.280 eV (See Fig. 6). We confirmed the transition state by calculating the vibrational frequency, which gave an imaginary frequency of 915.736 $cm^{-1}$. The calculation suggests that on adsorption formic acid will be physisorbed with appreciable dissociation.

**Table 4**
Adsorption energy of formate and formate co-adsorbed with a H atom on Cu(*h,k,l*) surface using PW91, PBE, PBE-D2 and PBEsol exchange-correlation functional.

| Systems | Adsorption energy (eV) | | | |
|---|---|---|---|---|
| Formate on $Cu_{3\times3}$ | | | | |
| | PBE | PE-D2 | P91 | PBEsol |
| Cu100 | −2.897 | −3.255 | −3.005 | −3.195 |
| Cu110 | −3.125 | −3.434 | −3.236 | −3.443 |
| Cu111 | −2.654 | −3.083 | −2.764 | −3.010 |
| Formate co-adsorbed with H atom on $Cu_{3\times3}$ | | | | |
| Cu100 | −0.639 | −1.054 | −0.692 | −1.003 |
| Cu110 | −0.868 | −1.228 | −0.932 | −1.182 |
| Cu111 | −0.483 | −0.990 | −0.543 | −0.906 |
| Formate co-adsorbed with H atom on $Cu_{4\times4}$ | | | | |
| Cu100 | −0.640 | −1.063 | −0.693 | −1.024 |
| Cu110 | −0.865 | −1.226 | −0.924 | −1.170 |
| Cu111 | −0.460 | −0.964 | −0.521 | −0.881 |

### 3.3. Geometry of formate on Cu(h,k,l)

We first considered the geometry of formate on Cu(111), Cu(110) and Cu(100) as predicted by PW91, PBE, PBE-D2 and PBEsol exchange-correlation functionals. As shown in Table 1 all the exchange-correlation functional considered in this study predicted comparable bond lengths for Cu–O, O–C, C–H which are close to the previously reported values [12,18]. The non-bonded OH distances in the O–C–H fragment were also considered for comparative purposes. The O–Cu bond lengths showed that inclusion of dispersion corrections in PBE-D2 resulted in shortening of the O–Cu bond lengths only slightly (0.010 Å – 0.038 Å) as compared to PBE predicted bond lengths.

These results show that while all these functionals predicts very similar geometries for the intramolecular distances of the organic fragment and, for the ligand–metal interatomic distances on the

**Table 5**
Bader charge analysis for Cu surfaces and on O, C and H atoms of formate as calculated using PW91, PBE, and PBEsol for the $Cu_{4\times4}$ models.

| Average Bader Charges (e-) | | | | | | | | | | | | |
|---|---|---|---|---|---|---|---|---|---|---|---|---|
| XC | | PW91 | | | | PBE | | | | PBEsol | | |
| System | Cu (srf) | O | C | H | Cu (srf) | O | C | H | Cu (srf) | O | C | H |
| Cu(100) | 0.036 | −1.582 | 2.354 | 0.133 | 0.036 | −1.577 | 2.352 | 0.127 | 0.041 | −1.126 | 1.541 | 0.082 |
| Cu(110) | 0.058 | −1.667 | 2.369 | 0.324 | 0.058 | −1.665 | 2.375 | 0.311 | 0.054 | −1.124 | 1.515 | 0.117 |
| Cu(111) | 0.034 | −1.582 | 2.370 | 0.139 | 0.034 | −1.583 | 2.374 | 0.139 | 0.034 | −1.125 | 1.528 | 0.110 |

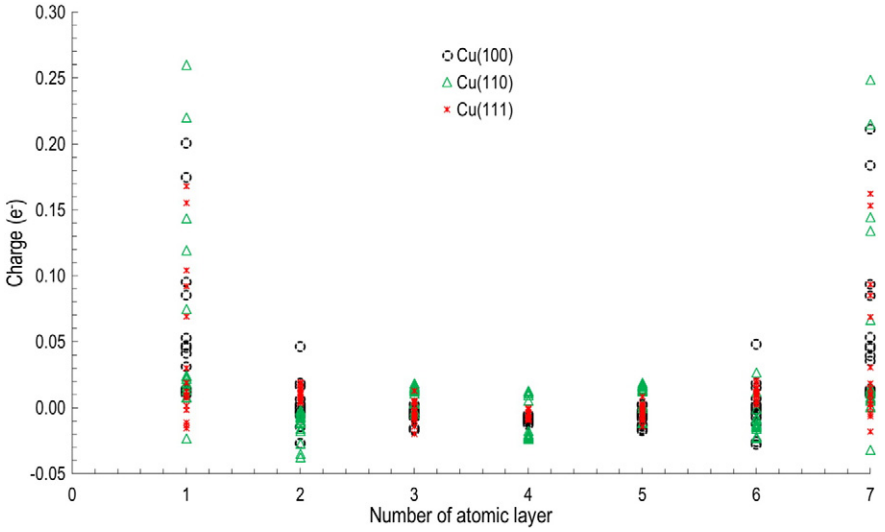


**Fig. 8.** Distribution of charges on Cu atoms in each layers of the $Cu_{4\times4}$ models. The dotted circles, empty triangle and red crosses represent Cu(100), Cu(110) and Cu(111) surfaces respectively.

surfaces, the PBEsol and PBE-D2 corrections predict slightly shorter distances than PW91 and PBE. It was also seen that O–Cu bond lengths are in the order of Cu(111) > Cu(100) > Cu(110), which also agrees very well with previous reports on formate adsorption on Cu low index surfaces on cluster models [18].

In realistic systems, the adsorption of formate may be accompanied by co-adsorption of H atoms. Therefore, we also considered the same models with a H atom co-adsorbed along with the formate. The H atom on Cu(111), Cu(110) and Cu(100) surfaces was adsorbed on 3-fold fcc, 4 fold hcp and the short bridged site respectively. For all of these models, the bond lengths calculated using PW91, PBE, PBE-D2 and PBEsol followed similar trends as described above. It is interesting to note that for the adsorbed H atom also, PW91 and PBE functionals predicted similar distances from the neighbouring Cu atoms. However, PBE-D2 and PBEsol functional predicted only slightly shorter Cu–$H_{adsorbed}$ distances (by ~0.013 Å) (see Table 2). Furthermore, as shown in Fig. 7, to investigate the influence of surface area coverage on bond lengths, we also considered another set of Cu 4 × 4 models with the formate molecule co-adsorbed with an H atom. These models also showed similar trends (see Table 3).

From this study, we conclude that irrespective of the surface coverage the trends of the bond lengths as predicted by PW91, PBE, PBE-D2 and PBEsol exchange-correlation did not change.

### 3.4. Adsorption energy of formate on Cu(h,k,l) surfaces

The calculated adsorption energies using (1) and (2) for formate on Cu(*h*,*k*,*l*) surfaces are summarized in Table 4. On analysing the calculated adsorption energy values, we find that, for all the models, the adsorption energy for formate on the Cu(110) surface was the most negative i.e., it is lower in energy than formate on Cu(100) and Cu(111) surfaces by −0.228 eV and −0.471 eV respectively. All the exchange-correlation functionals predicted similar trends. For formate co-adsorbed with an H atom on Cu(*h*,*k*,*l*) the adsorption energies for the $Cu_{3\times3}$ and $Cu_{4\times4}$ models were comparable. In the next step of this study we analysed various electronic properties such as Bader charge, charge density and partial density of states (PDOS) of these systems to clarify the underlying reason for the relatively higher stability of formate on Cu(110) surfaces.

### 3.5. Bader charge analysis and charge density

For a deeper understanding of the nature of electronic interaction between formate and Cu(*h*,*k*,*l*) surfaces, we performed Bader analyses. First, we calculated the average charge distribution on the Cu surfaces using PW91, PBE, and PBEsol exchange-correlation functionals. We find that, the average surface Cu charges on Cu(110), as predicted by

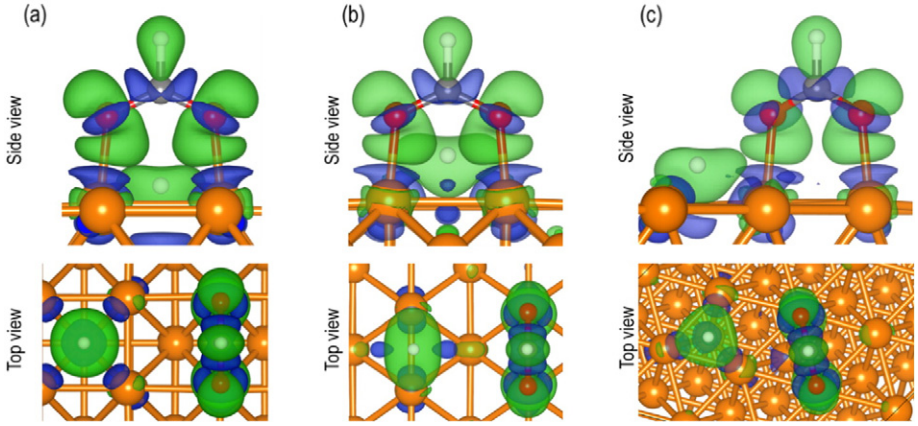


**Fig. 9.** Side and top view of isosurface (0.002e/Å$^3$) of electron charge density of formate coadsorbed with H atom on (a) Cu(100), (b) Cu(110) and (c) Cu(111) surfaces.

PW91 and PBE exchange-correlation functionals are 0.02 $e^-$ more positive than Cu(100) and Cu(111) surfaces (see Table 5), i.e., the charge transferred by the Cu(110) surface is comparatively higher than on the other two surfaces. As shown in Fig. 8, we also performed an analysis of the charge distribution layer-by-layer for each atom of the Cu surfaces and sub-surfaces; showing the Cu(110) surface had the most positive charges i.e., Cu(110) surfaces favour more electron transfer as compared to the other surfaces. On carefully analysing the data, we find traces of negative charges on some Cu surface atoms. Traces of positive and negative charges are also seen on the Cu sub-surfaces. To clarify this point further, we calculated the electron density of the systems using equation (3). The green lobes on Cu and O atoms of formate show electron loss from both $O_{formate}$ and Cu bonded to the $O_{formate}$. As shown in Fig. 9, the blue lobes in the interfacial region between the formate molecule and Cu surface may be the result of the accumulation of charge from the Cu surface and formate. Even though we did not see any direct correlation between the accumulation of electron density at the interfacial region and the trend of calculated adsorption energies, it is interesting to note that there is a bidirectional electron transfer (BiDET) from Cu surfaces as well as from the formate. We also analysed the charge on the O, C and the H atoms of formate and we find that they are comparable on different surfaces. These charge values suggest small local charge redistribution between formate and the Cu surfaces. The study using Bader charge and electron density suggests that higher charge transfer from Cu(110) surface and an optimum electron density due to BiDET might favour higher stability of formate on this surface as compared to the Cu(100) and Cu(111) surfaces.

### 3.6. Molecular orbital interactions and stability of formate

We also analysed the atom projected partial density of states (PDOS) to understand the trend in the adsorption energies. As shown in Fig. 10, in the partial density of states for all the models, the region immediately below the Fermi energy ($E_F$) was dominated by the highly localized Cu *d*-orbital. The signatures due to the O *p* orbitals also appeared just below $E_F$, which is the case for all the models. On further analysing the

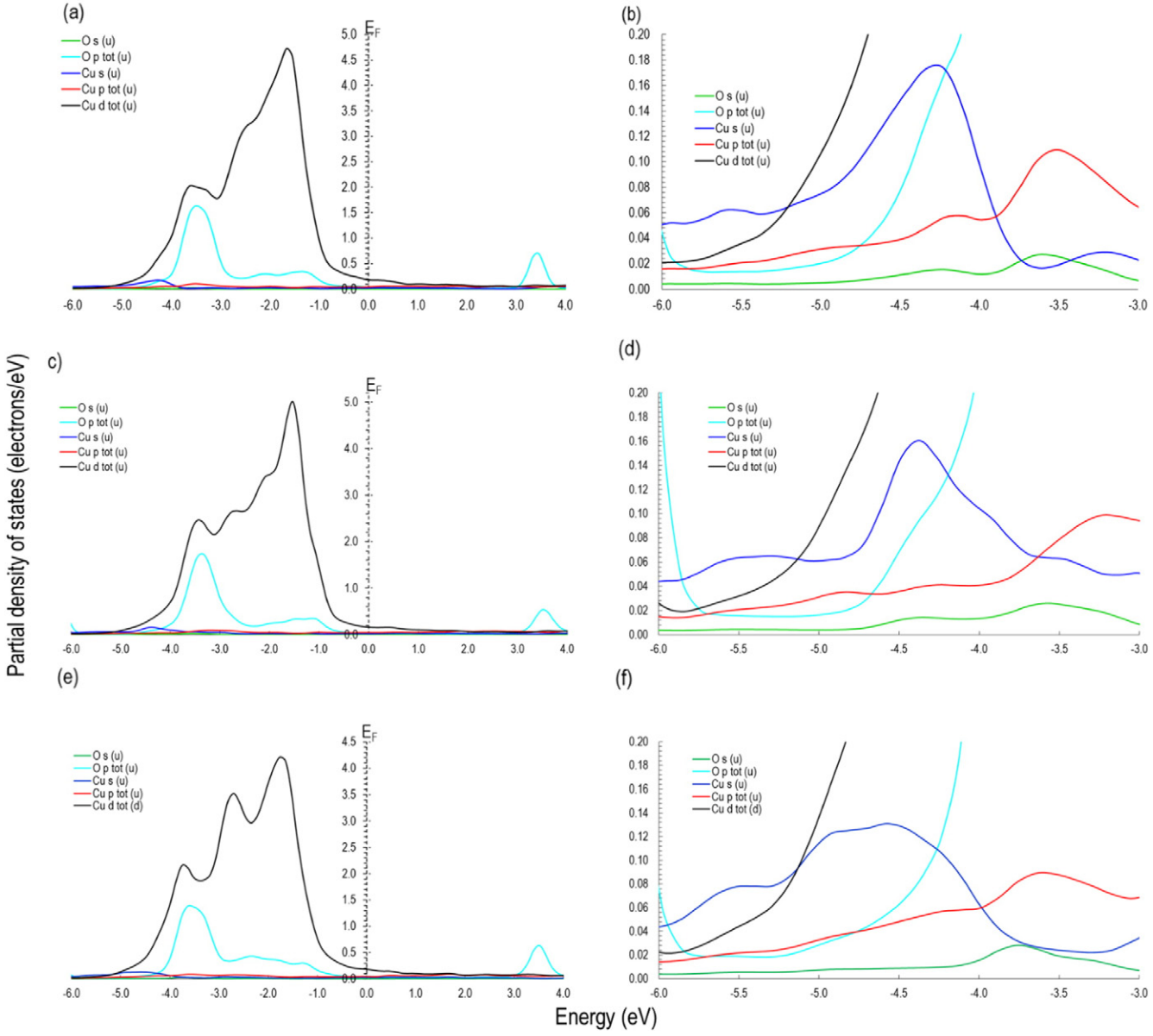


**Fig. 10.** Partial density of states for $O_{formate}$ and Cu atom bonded to it (a) for Cu(100) surface, (b) in the enlarged area around −6.0 to −4.0 eV for Cu(100) surface, (c) for Cu(110) surface, (d) in enlarged area around −6.0 to −4.0 eV for Cu(110) surface, (e) for Cu(111) surface and (f) in the enlarged area around −6.0 to −4.0 eV for Cu(111) surface. "u" in the parenthesis refers to up-spin PDOS. Since the up-spin and down-spin PDOS are similar only up-spin PDOS is shown.

orbital interactions below the Fermi energy, we find that at around –5.5 eV to –4.0 eV there is crossing and overlapping of signatures due to the O (*s*, *p*) and Cu (*s*, *p*) orbitals. For clarity, we have further enlarged the area around this region (see Fig. 10b, d and f). So the nature of these orbitals around this region determines the nature of the bonding between Cu and O, which is however, similar for all the models. Therefore, to understand the trend in adsorption energies, we investigated the nature of the Cu *d* orbitals in this region. To highlight the highest contribution of individual *d*–orbitals, we further deconvoluted the *d* orbital signatures (Fig. 11(a-c)), from which we see that for formate adsorbed on the Cu(111) surface, all the *d*-orbitals (i.e., $d_{xy}$, $d_{yz}$, $d_{z^2}$, $d_{xz}$, and $d_{x^2-y^2}$) in −5.5 to −4.0 eV overlap. Clearly, all the *d* orbitals are hybridized to form strong bonds. However, on the Cu(100) and Cu(110) surfaces, the *d*-orbitals around this region are dispersed leaving the possibility of hybridization between O (*s*, *p*) and Cu (*s*, *p*, *d*) to form relatively stronger bonds between them explaining the reason for the lower adsorption energy of formate molecule on Cu(100) and Cu(110) surfaces as compared to the Cu(111) surface. On further investigating the Cu *d*–orbitals for Cu(100) and Cu(110) surfaces around this region, we see that in the case of Cu(100) surfaces, the signatures due to $d_{z^2}$ and $d_{x^2-y^2}$ make the largest contribution, while in the case of Cu(110) surface the highest contribution is made by $d_{yz}$ and $d_{xz}$. However, in an octahedral-like crystal field splitting, the axial $d_{z^2}$ and $d_{x^2-y^2}$ orbitals have higher energy making it less favourable for bonding between $O_{formate}$ and Cu atoms as compared to the non-axial $d_{yz}$ and $d_{xz}$ orbitals. This analysis clearly explains the trend in adsorption energy and hence the stability of formate on Cu(*h*,*k*,*l*) surfaces as $Cu(110)_{formate} > Cu(100)_{formate} > Cu(111)_{formate}$.

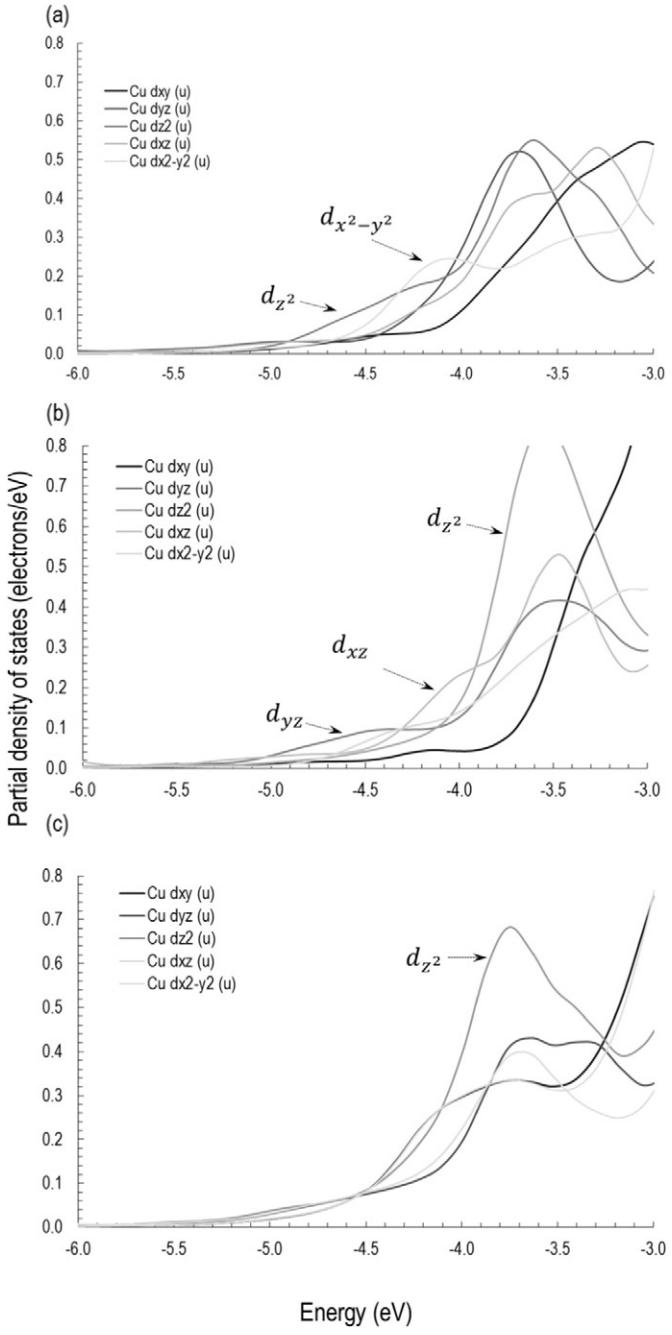


**Fig. 11.** Partial density of states for Cu d orbitals in −6.0 to −4.0 eV energy region for (a) Cu(100), (b) Cu(110) and (c) Cu(111) surfaces. "u" in the parenthesis refers to up-spin PDOS. Since the up-spin and down-spin PDOS are similar only up-spin PDOS is shown.

### *3.7. Geometry and electronic properties of formate in the presence of a positive ion*

Another point to note is that in this study and in previous studies formate has been modelled as a free radical [12]. But it is important to consider if there is any influence of charge localisation in the formate on the adsorption energy trends. However, it is not straightforward to model charged species with periodic boundary conditions [39]. Therefore, as noted earlier we performed another set of calculations on $Cu_{4\times4}$ (111, 110 and 100) surfaces by placing a positive $Na^+$ ion nearby the formate on a three-fold hollow site, long-bridge site and four-fold hollow site for Cu(111), Cu(110) and Cu(100) surfaces respectively (See Fig. S1).

In these calculations, the calculated bond lengths for O–Cu, O–C, C–H bulk and surface Cu–Cu are close to those of the calculations performed on formate co-adsorbed with a H atom on $Cu_{4\times4}$ (111, 110 and 100) surfaces (See Table S1). The trend in adsorption energies of these system and hence the stability of formate also remains the same [i.e., $Cu(110)_{formate}$ (with $E_{ad} = -5.014$ eV) > $Cu(100)_{formate}$ (with $E_{ad} = -4.702$ eV) > $Cu(111)_{formate}$ (with $E_{ad} = -4.424$ eV)]. The analysis on Bader charges shows (See Table S2 and Fig. S2) that the average charges on Cu atoms on Cu(111, 110 and 100) surfaces become slightly electron rich, which we found when we analysed the distribution of charges on Cu atoms in each layer of these models (Fig. S2). The Cu atoms closer to the $Na^+$ ion are more negative than the atoms closer to the formate. Additionally, we also see that the Cu atoms closer to the formate on Cu(110) surface are relatively more positive than the other two surfaces. The charges on O atoms are close with the values as obtained for formate and H co-adsorbed models. Further, on comparing the charges on C atoms we see that on these systems with a $Na^+$ ion the carbon atom is approximately 0.817 $e^-$ less positive, which means that formate is anionic in nature. Irrespective of the nature of formate i.e., neutral or anionic form the geometry and relative adsorption energies on Cu(111, 110 and 100) surface do not alter significantly.

## 4. Summary

We performed a systematic study of the stability of formate on Cu(*h*,*k*,*l*) surfaces. A comparison of the calculated vibrational transition energies of a perpendicular configuration of formate on a Cu surface shows excellent agreement with the experimental spectrum obtained from inelastic neutron spectroscopy. The geometric and electronic properties were investigated at the PW91, PBE, PBE-D2 and PBEsol level of theory. We find that these functionals predict similar geometries for formate adsorbed on the Cu surface irrespective of the surface coverage. The calculations of adsorption energy show that formate species is more stable on the Cu(110) surface as compared to Cu(111) and Cu(100) surfaces. To clarify the trends in adsorption energy an analysis on Bader charges and atom projected partial density of states were carried out. The Bader analysis shows that the greater adsorption energy of the Cu(110) surface could be related to the larger charge transfer

from the Cu surface atoms. The charges on formate species differ depending on whether it is adsorbed as a radical or as an anion. However, the geometries and relative adsorption energies are largely unchanged by it. Interesting bidirectional electron transfer between formate and the Cu surfaces are also observed. The analysis of the partial density of states shows that at around the –5.5 eV to –4.0 eV region, hybridization between O *p* and the non-axial Cu $d_{yz}$ and $d_{xz}$ orbitals takes place in Cu(110) surface, which is energetically favourable and hence formate is more stable on Cu(110) surface. This work in conjugation with INS experiments provides a detailed theoretical insight into the stability of formate on Cu(*h*,*k*,*l*) surfaces.

## Acknowledgments

Via our membership of the UKs HEC Materials Chemistry Consortium, which is funded by EPSRC (EP/L000202), this work used the ARCHER UK National Supercomputing Service (http://www.archer.ac.uk). The STFC Rutherford Appleton Laboratory is thanked for access to neutron beam facilities. The UK Catalysis Hub is thanked for resources and support provided via our membership of the UK Catalysis Hub Consortium and funded by EPSRC (grants EP/K014706/1, EP/K014668/1, EP/K014854/1, EP/K014714/1 and EP/M013219/1).

## Appendix A. Supplementary data

Supplementary data to this article can be found online at http://dx.doi.org/10.1016/j.susc.2016.05.002.

## References

[1] J.A. Rodriguez, S.D. Senanayake, D. Stacchiola, P. Liu, J. Hrbek, Acc. Chem. Res. 47 (2014) 773.
[2] M. Bowker, E. Rowbotham, F.M. Leibsle, S. Haq, Surf. Sci. 349 (1996) 97.
[3] L. Romaner, G. Heimel, J.-L. Brédas, A. Gerlach, F. Schreiber, R.L. Johnson, J. Zegenhagen, S. Duhm, N. Koch, E. Zojer, Phys. Rev. Lett. 99 (2007) 256801.
[4] R.J. McCarty, J. Falconer, R.J. Madix, J. Catal. 30 (1973) 235.
[5] M. Bowker, R.J. Madix, Surf. Sci. Lett. 102 (1981) A18.
[6] I.E. Wachs, R.J. Madix, Surf. Sci. 84 (1979) 375.
[7] S. Poulston, R.A. Bennett, A.H. Jones, M. Bowker, Surf. Sci. 55 (1997) 888.
[8] A.H. Jones, S. Poulston, R.A. Bennett, M. Bowker, Surf. Sci. 380 (1997) 31.
[9] T.G.A. Youngs, S. Haq, M. Bowker, Surf. Sci. 602 (2008) 1775.
[10] M.D. Crapper, C.E. Riley, D.P. Woodruff, Surf. Sci. 171 (1986) 1.
[11] S. Poulston, R.P. Holroyd, M. Bowker, S.F. Parker, P.C. Mitchell, Surf. Sci. 402-404 (1998) 599.
[12] N. Atodiresei, K. Schroeder, S. Blügel, Phys. Rev. B Condens. Matter Mater. Phys. 75 (2007) 1.
[13] J.R.B. Gomes, J.A.N.F. Gomes, Surf. Sci. 432 (1999) 279.
[14] H. Nakatsuji, M. Yoshimoto, Y. Umemura, S. Takagi, M. Hada, J. Phys. Chem. 100 (1996) 694.
[15] J.M. Phillips, F.M. Leibsle, A.J. Holder, T. Keith, Surf. Sci. 545 (2003) 1.
[16] M. Sambi, G. Granozzi, M. Casarin, A. Rizzi, A. Vittadini, S. Caputi, G. Chiarello, Surf. Sci. Lett. 315 (1994) 309.
[17] H. Ma, G. Wang, Y. Morikawa, J. Nakamura, Sci. China Ser. B Chem. 52 (2009) 1427.
[18] H. Zhenming, R.J. Boyd, J. Chem. Phys. 112 (2000) 9562.
[19] K. Morikawa, Y. Iwata, K. Nakamura, J. Terakura, Chem. Phys. Lett. 304 (1999) 91.
[20] G. Kresse, J. Hafner, Phys. Rev. B 47 (1993) 558.
[21] G. Kresse, J. Hafner, Phys. Rev. B 49 (1994) 14251.
[22] G. Kresse, J. Furthmüller, Phys. Rev. B 54 (1996) 11169.
[23] P.E. Blöchl, Phys. Rev. B 50 (1994) 17953.
[24] J.P. Perdew, K. Burke, M. Ernzerhof, Phys. Rev. Lett. 77 (1996) 3865.
[25] H.M. Otte, J. Appl. Phys. 32 (1961) 1536.
[26] J.P. Perdew, Y. Wang, Phys. Rev. B 45 (1992) 13244.
[27] J.P. Perdew, A. Ruzsinszky, G.I. Csonka, O.A. Vydrov, G.E. Scuseria, L.A. Constantin, X. Zhou, K. Burke, Phys. Rev. Lett. 136406 (2007) 4.
[28] S. Grimme, J. Comput. Chem. 27 (2006) 1787.
[29] X.-Y. Pang, L.-Q. Xue, G.-C. Wang, Langmuir 23 (2007) 4910.
[30] K. Nobuhara, H. Nakanishi, H. Kasai, A. Okiji, Surf. Sci. 493 (2001) 271.
[31] J.L. Nie, H.Y. Xiao, X.T. Zu, Chem. Phys. 321 (2006) 48.
[32] W. Tang, E. Sanville, G. Henkelman, J. Phys. Condens. Matter 21 (2009) 084204.
[33] G. Henkelman, B.P. Uberuaga, H. Jónsson, J. Chem. Phys. 113 (2000) 9901.
[34] G. Henkelman, H. Jónsson, J. Chem. Phys. 113 (2000) 9901.
[35] G. Makov, M. Payne, Phys. Rev. B 51 (1995) 4014.
[36] J. Neugebauer, M. Scheffler, Phys. Rev. B 46 (1992) 16067.
[37] S.J. Clark, M.D. Segall, C.J. Pickard, P.J. Hasnip, M.J. Probert, K. Refson, M.C. Payne, Z. Krist. 220 (2005) 567.
[38] A.J. Ramirez-Cuesta, Comput. Phys. Commun. 157 (2004) 226.
[39] H.-P. Komsa, A. Pasquarello, Phys. Rev. Lett. 110 (2013) 1.